Peer-reviewed version available at *Materials* **2019**, *12*, 3012; doi:10.3390/ma12183012

Article

Hexacyano ferrate (III) reduction by electron transfer induced by plasmonic catalysis on gold nanoparticles

Iyad Sarhid,[1] Isabelle Lampre,[1,*] Diana Dragoe,[2] P. Beaunier,[3] Bruno Palpant,[4] Hynd Remita[1,5,*]

[1] Laboratoire de Chimie Physique, UMR 8000 Université Paris-Sud / CNRS, Université Paris-Saclay, 91405 Orsay, France; iyad.sarhid@u-psud.fr (I.S.); Isabelle.lampre@u-psud.fr (I.L.)
[2] Institut de Chimie Moléculaire et des Matériaux, UMR 8182 Université Paris-Sud / CNRS, Université Paris-Saclay, 91405 Orsay, France ; diana.dragoe@u-psud.fr (D.D.)
[3] Sorbonne Université, CNRS, UMR 7197, LRS, 4 Place Jussieu, Paris 75005, France; patricia.beaunier@sorbonne-universite.fr (P.B.)
[4] Laboratoire de Photonique Quantique et Moléculaire, UMR 8537 CentraleSupélec / Ecole Normale Supérieure Paris-Saclay / CNRS, Université Paris Saclay, 91190 Gif-sur-Yvette, France; bruno.palpant@centralesupelec.fr (B.P.)
[5] CNRS, Laboratoire de Chimie Physique, UMR 8000 Université Paris-Sud, Université Paris-Saclay, 91405 Orsay, France ; hynd.remita@u-psud.fr (H.R.)
* Correspondence: hynd.remita@u-psud.fr (H.R.)

Abstract: Redox reactions are of great importance in environmental catalysis. Gold nanoparticles (NPs) have attracted much attention because of their catalytic activity and their localized surface plasmon resonance (LSPR). In the present study, we investigated in details the reduction of ferricyanide (III) ion into ferrocyanide (II) ion catalyzed by spherical gold nanoparticles of two different sizes 15 nm and 30 nm and excited at their LSPR band. Experiments were conducted in the presence (or not) of sodium thiosulfate. This catalysis is enhanced in the presence of Au-NPs under visible light excitation. This reduction takes also place even without sodium thiosulfate. Our results demonstrate the implication of hot electrons in this reduction.

Keywords: Catalysis; Ferricyanide (III) reduction; Plasmon resonance; Gold nanoparticles; Electron transfer.

1. Introduction

Redox reactions are of great importance in environmental catalysis as, for example, reduction of nitrogen oxides (deNOx), CO_2 or heavy metals, and generation of hydrogen from water or oxidation of CO or organic pollutants [1]. Platinum, palladium and rhodium are the most used metal catalysts in hydrogenation reactions or in catalytic convertors for deNOx and CO reduction [2]. Catalysis by gold is a domain of increased interest since the discovery by Haruta [3] that small gold nanoparticles (Au-NPs) can catalyze CO reduction at room temperature [4-9].

(Au-NPs) have also attracted much attention due to their localized surface plasmon resonance (LSPR), *i.e.*, the oscillations of metal free electrons driven by the electric field of the incident light. There are many applications utilizing the SPR of gold nanoparticles, including subwavelength electromagnetic energy transport, chemical and biological sensors [1,6,10], surface enhanced Raman scattering (SERS) [11,12], plasmonic photocatalysis [13-15], and photothermal cancer therapy [16-19], where the plasmonic energy is converted locally into heat that raises the surrounding medium temperature, leading to cancer cell killing. In thermal therapy, hot electrons induced by surface plasmon excitation, lead (after reaction with oxygen or water) to formation of reactive oxygen species (ROS) ($HO^{\cdot}$, $O_2^{\cdot -}$ and singlet oxygen), which are also responsible in cancer cell killing [20].

Metal nanoparticles such as gold and platinum NPs are efficient catalysts in different reactions with environment applications. These catalytic reactions often involve electron transfers [21,22].

Peer-reviewed version available at *Materials* **2019**, *12*, 3012; doi:10.3390/ma12183012

Reduction of ferrocyanate (III) has been taken as a model reaction to study catalysis by metal NPs [21-23].

Mulvaney, *et al* [23] studied redox catalysis by colloidal gold for the reduction of ferricyanide (III) ions by borohydride ions in alkaline aqueous solution. They found that Au-NPs dramatically increase the reaction rate and that Au-NPs also change the mechanism: The reaction is zero order in hexacyanoferrate (III) concentration for the non-catalyzed reaction to first order for the catalyzed reaction. In this reaction, the Au-NPs act as a reservoir for the electrons and become cathodically polarized. In a first step, borohydride can inject electrons onto Au-NPs, then ferricyanide ions diffuse to the nanoparticle surface and are reduced by excess surface electrons. These nanoparticles serve as a relay for electrons.

El Sayed's group reported on catalysis by metal nanoparticles for the reduction of ferricyanide ion by thiosulfate to ferrocyanide [22,24,25]:

$$2Fe(CN)_6^{3-} + 2S_2O_3^{2-} \rightarrow 2Fe(CN)_6^{4-} + S_4O_6^{2-}.$$

This reaction has been used to compare the catalytic activity of different nanoparticles. Size and shape dependent catalytic activity of platinum nanoparticles for this reaction has been demonstrated [22,26]. The study conducted on tetrahedral, cubic and spherical Pt nanoparticles has demonstrated that the kinetic parameters correlate with the fraction of surface atoms located on the corners and edges in each size and shape [26]. It has been also demonstrated that Au-NPs are very efficient catalysts for the reduction of ferricyanide (III) ion to ferrocyanide. El-Sayed *et al*. reported that catalysis of this reaction by gold nanoparticles was enhanced when the latter were irradiated at their plasmon wavelength [22]. The value of the activation energy of this electron transfer reaction for two different shapes of Au-NPs (nanospheres and nanocages) was measured. This activation energy was found to be similar when using a thermostatic water bath or by using a plasmonic photothermal reactor. This result supported the conclusion that the role of the surface plasmon field on the electron dynamics during the reaction was negligible, and that the main effect was due to temperature increase after plasmon excitation [7,14,15].

Recently, the LSPR effect of plasmonic nanostructures has been successfully applied to photocatalysis under visible light irradiation and proved to be very promising [14,27,28].

In the present study, we investigated in details the reduction of ferricyanide (III) ion into ferrocyanide (II) ion catalyzed by spherical Au-NPs and excited at their LSPR band. Experiments were conducted in the presence (or not) of sodium thiosulfate. This catalysis is enhanced in the presence of Au-NPs with light excitation. We show for the first time that this reduction takes place even without sodium thiosulfate demonstrating the implication of hot electrons in this reduction.

2. Materials and Methods

Tetrachloroauric acid ($HAuCl_4.3H_20$), trisodium citrate trihydrate, potassium hexacyanoferrate (III) (HC-FeIII), sodium thiosulfate (ST) and *para*-nitrothiophenol (pNTP) of high purity were purchased from Aldrich and used as received. All the experiments were carried out with Milli-Q water with resistivity higher than 18 MΩ cm.

Spherical Au-NPs were synthesized by Türkevich method [29-31]. An aqueous solution of $HAuCl_4$ is heated to the boiling point in an Erlenmeyer, and then, a sodium citrate aqueous solution is added with vigorous magnetic stirring. This solution is heated during about 10 min, and the red solution obtained is left cooling. Two well-defined sizes of Au-NPs (Au-NPs@citrate) were obtained by changing the experimental conditions. Au-NPs with mean diameters of 15 and 30 nm respectively were obtained with a concentration ratio of citrate to gold equal to 6.8 and 1.4, respectively, and an initial concentration of gold ions, [Au^{III}], of 0.25 mM and 1 mM, respectively [30]. The 30 nm-Au-NPs@citrate solutions were then diluted by a factor of four to get the same concentration of Au atoms as in the 15 nm-Au-NPs@citrate solutions.

15 nm (30 nm) Au-NP@citrate colloidal solutions were produced by adding 1 mL (0.8 mL) of an aqueous solution of trisodium citrate (34 mM, 1 wt%) to 20 mL of a stirred boiling aqueous solution of $HAuCl_4$ of concentration 0.25 mM (1 mM)[31]. Then, to change the stabilizing agent, aqueous solutions of pNTP (6×10^{-4} M) were prepared, and the pH was adjusted to 11 by addition of 0.1 M NaOH solution in order to form the phenolate anion

Then, 750 µL of an alkaline pNTP solution were added to 2 mL of AuNP solutions contained in a 1 cm square cuvette. Following that, the solutions were left under continuous stirring in the dark for 40 minutes to ensure the adsorption of pNTP and replacement of citrate on the surface of Au-NPs.

For the catalytic reactions under irradiation, sodium thiosulfate and hexacyano-ferrate (III) were added to a solution containing Au-NPs. The final concentrations for each reagent were: sodium thiosulfate: 10^{-3} M, hexacyano-ferrate (III): 10^{-3} M, Au-NPs: 0.25×10^{-3} M (concentration in Au atoms). 2 mL of the mixture were introduced in a quartz cell with an optical path of 1 cm (and containing a small magnetic rod). The cell was properly sealed, bubbled with N_2 for 20 minutes to get rid of O_2, and then irradiated under stirring either with LEDs at $\lambda = 520$ nm (home reactor, Figure S1) or with an Oriel 300 W Xenon lamp equipped with an infrared water filter and an optical cutoff filter (longpass filter GG450, $\lambda > 450$ nm) to avoid the direct excitation of ferrocyanide (III) ion, which absorbs in the range 350-400 nm (Figure S2**)**.

The UV-visible absorption spectra were recorded using a HP8543 spectrophotometer and were used to follow the reaction kinetics.

The size and shape of Au-NPs before and after catalytic reactions were characterized by Transmission Electron Microscopy (TEM) using a JEOL JEM 100CX microscope operating at an accelerating voltage of 100 kV. Few drops of the samples (which were first sonicated to disperse precipitated aggregates when necessary) were deposited on carbon coated copper grids and dried under N_2 flow. TEM images were taken from different sections of the TEM grid to verify the size and shape distributions of the nanoparticles.

XPS analysis was performed using a K Alpha instrument from Thermo Fisher, with a monochromatic $Al_{K\alpha}$ X-ray source (1486.7 eV) and a hemispherical analyzer, at a take-off angle of 0°. Films of the samples were drop-cast on thoroughly cleaned silica plates. The wide scan spectra were acquired at a pass energy of 200 eV and an energy step of 1 eV, while the narrow scan spectra at 50 eV pass energy and 0.1 eV energy step. Charge correction was accomplished by means of a dual beam source. The binding energy scale was checked against neutral C1s, set at 284.8 eV. Binding energies are given with a precision of ± 0.2 eV. The spectra obtained were treated by means of Avantage software, provided by the manufacturer. A Shirley background subtraction was used and the peak areas were normalized using the Scofield sensitivity factors. Mixed Gaussian-Lorentzian (GL) functions (30% L) were used as line shapes in spectral decomposition, with asymmetry added to the metallic Au core-level spectrum.

3. Results

We have investigated the catalytic properties of Au-NPs under plasmon excitation on the reduction of HC-FeIII in the presence or in the absence of the reducing partner ST. Figure 1 shows the UV-visible spectra and TEM images of the synthesized and used Au-NPs@citrate with two different main diameters of 15 and 30 nm. The maximum of the LSPR band is located at 515 and 525 nm for the solutions containing Au-NPs of a mean size of 15 and 30 nm respectively.

Peer-reviewed version available at Materials 2019, 12, 3012; doi:10.3390/ma12183012

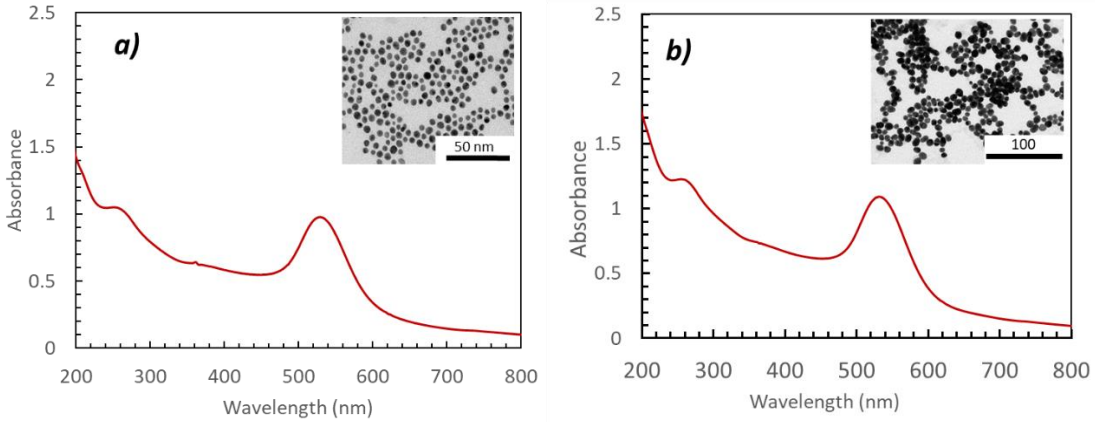

Figure 1. UV-Visible spectra and inset TEM images of the spherical gold nanoparticles synthesized by citrate reduction: (**a**) 15 nm-AuNPs@citrate and (**b**) 30 nm-AuNPs@citrate. Optical path length: 1 cm.

3.1. Reduction of hexacyanoferrate in the presence of sodium thiosulfate

The studied reaction is the reduction of ferricyanide or hexacyanoferrate, HC-FeIII, by thiosulfate:

$$2\ Fe(CN)_{6\,(aq)}^{3-} + 2\ S_2O_{3\,(aq)}^{2-} \rightarrow\ 2\ Fe(CN)_{6\,(aq)}^{4-} + S_4O_{6\,(aq)}^{2-} \quad (1)$$

The redox potential of the couples involved in this reaction are $E^0(Fe(CN)_6^{3-}/Fe(CN)_6^{4-}) = +0.36$ V and $E^0(S_4O_6^{2-}/S_2O_3^{2-}) = +0.08$ V versus the normal hydrogen electrode at 25°C [32]. Although thermodynamically favorable, this reaction needs to be catalyzed. Solutions containing HC-FeIII and ST (without Au-NPs) are stable at room temperature, even under irradiation, while in the presence of Au-NPs and in the absence of irradiation, the reaction takes place as shown by the disappearance of the absorption bands at 310 and 420 nm associated to HC-FeIII (Figure 2). The rate of the reaction depends on the size of the Au-NPs.

Peer-reviewed version available at Materials 2019, 12, 3012; doi:10.3390/ma12183012

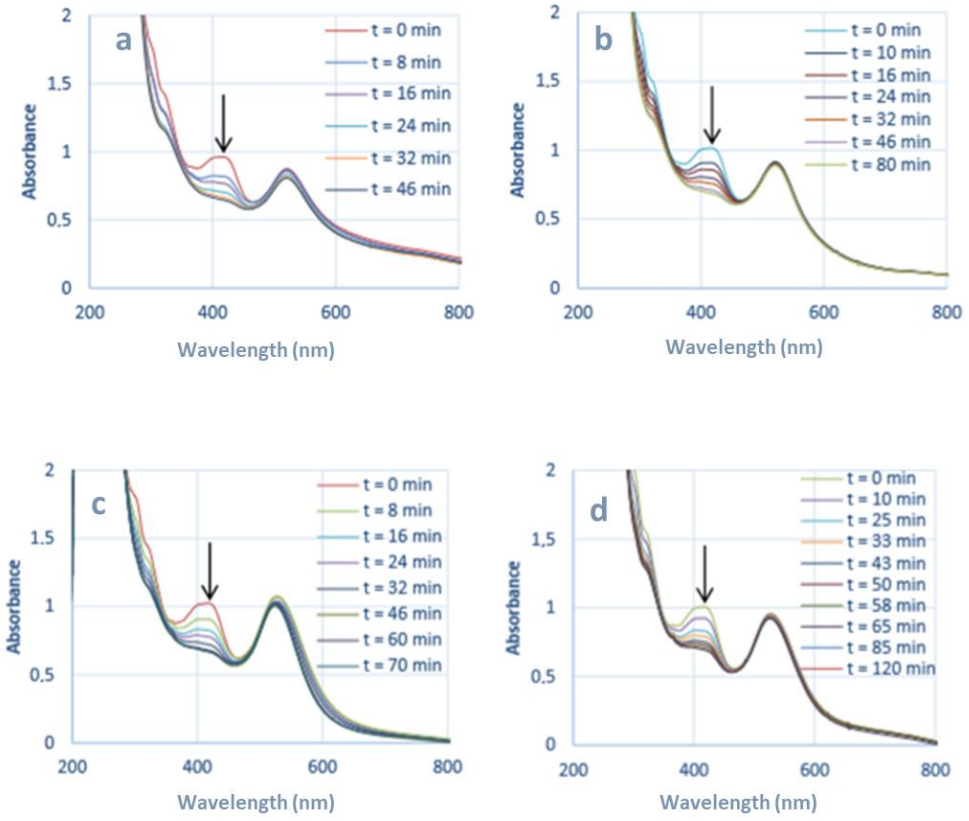

Figure 2. Spectral evolution with time of deaerated aqueous solutions containing 10^{-3} M sodium thiosulfate and 10^{-3} M potassium hexacyanoferrate: **(a)** in the presence of 15 nm Au-NPs@citrate in the dark, **(b)** in the presence of 15 nm Au-NPs@citrate under irradiation at λ = 520 nm, **(c)** in the presence of 30 nm Au-NPs@citrate in the dark, and **(d)** in the presence of 30 nm Au-NPs@citrate under irradiation at λ = 520 nm. Optical path length: 1 cm.

3.1.1. Irradiation using LEDs at λ = 520 nm

Figure 2 presents the spectral evolution of solutions containing HC-FeIII, ST and Au-NPs@citrate under LEDs irradiation at λ = 520 nm, close to the LSPR of Au-NPs. For both sizes of Au-NPs@citrate, the bands at 310 and 430 nm due to HC-FeIII decrease in intensity with irradiation time and disappear after about 45 and 60 minutes of irradiation for 15 nm and 30 nm Au-NPs@citrate, respectively. The LSPR band of the spherical Au-NPs (with a maximum around 515 nm or 525 nm for the solutions containing Au-NPs of 15 and 30 nm respectively) remains quite stable during the whole irradiation time indicating no drastic changes in the Au-NPs morphology.

The kinetics of the reduction reaction of HC-FeIII by ST is followed by the decrease in the absorbance at 420 nm (Figure 3). The reduction is faster for the smaller 15 nm Au-NPs@citrate compared to 30 nm Au-NPs@citrate, and for both sizes the reduction is accelerated by the irradiation. These results confirm that Au-NPs play a role of catalysts in this reaction. As catalysis takes place at the surface of the nanoparticles, the kinetics is enhanced with the specific surface area. Considering the average size of the nanoparticles (15 and 30 nm) and assuming that they are quasi-spherical, their specific surface areas are respectively 14.5 $m^2\ g^{-1}$ and 7.3 $m^2\ g^{-1}$, respectively. Moreover, the excitation of the LSPR of the Au-NPs favors the catalytic properties of the Au-NPs. This plasmonic effect could be related to different mechanisms:

Preprints (www.preprints.org) | NOT PEER-REVIEWED | Posted: 17 July 2019 doi:10.20944/preprints201907.0197.v1

Peer-reviewed version available at Materials 2019, 12, 3012; doi:10.3390/ma12183012

1. Electron density exchange between the excited gold nanoparticles and nearby reactants;
2. Effect of the plasmonic near field enhancement on the electron transfer process between HC-FeIII and ST;
3. Temperature increase due to a rapid conversion of the excited surface plasmon resonance into heat that would eventually accelerate the chemical reaction.

It is to note that the temperature increase in the solution during the reaction under irradiation was around 3-4 degrees as measured by a thermos-couple immersed inside the reaction cuvette, but the increase of temperature at the surface of nanoparticles (induced by plasmon resonance) is much higher. Under continuous irradiation, each NP contributes to the global warming of the solution they are surrounded by.

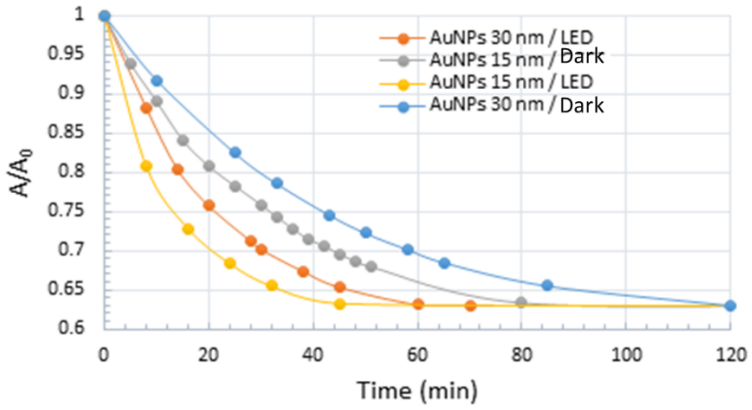

Figure 3. Kinetic trace of the normalized absorbance at 420 nm for the reduction of HC-FeIII in deaerated aqueous solutions containing 10^{-3} M sodium thiosulfate and 10^{-3} M potassium hexacyanoferrate in the presence of 15 nm or 30 nm Au-NPs@citrate in the dark or under LEDs irradiation at 520 nm.

3.1.2. Irradiation using a Xe lamp equipped with a 450 nm optical cutoff filter

Similar experiments were performed using a Xe lamp with a 450 nm optical cutoff filter instead of using the LEDs at 520 nm. Under these conditions, in addition to the disappearance of the absorption bands at 310 and 420 nm due to HC-FeIII, changes in the LSPR band of the Au-NPs@citrate are observed (Figure 4). For 15 nm Au-NPs@citrate, the LPSR band around 530 nm totally disappears simultaneously as the bands of HC-FeIII (Figure 4a) while for 30 nm Au-NPs@citrate, the LSPR band around 530 nm decreases partially and a new broad band with a maximum around 750 nm appears (Figure 4b). These results indicate that during the reduction reaction upon Xe lamp irradiation the morphology of the Au-NPs@citrate changes dramatically, what is confirmed by TEM images (Figure 5).

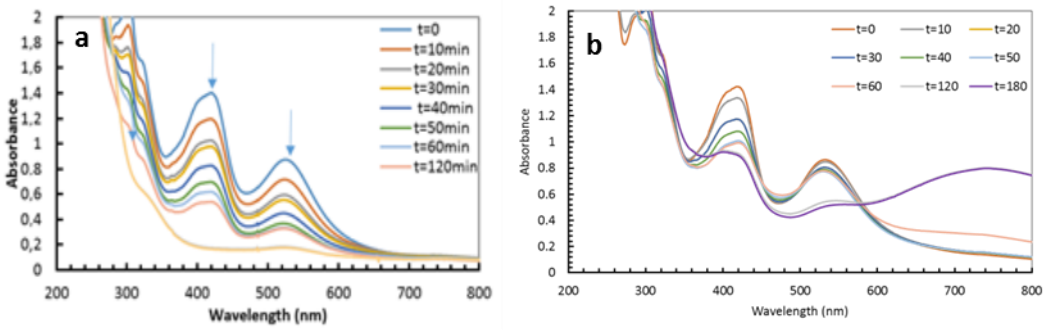

Figure 4. Spectral evolution with time of deaerated aqueous solutions containing 10^{-3} M sodium thiosulfate and 10^{-2} M potassium hexacyanoferrate under Xe lamp irradiation (equipped with an optical cutoff filter at 450 nm) (**a**) in the presence of 15 nm Au-NPs@citrate and (**b**) 30 nm Au-NPs@citrate. Optical path length: 1 cm.

Peer-reviewed version available at *Materials* **2019**, *12*, 3012; doi:10.3390/ma12183012

Figures 5 and 6 show TEM images of the Au-NPs present at different times during the reduction reaction under Xe lamp irradiation. The TEM images show that Au-NPs reshape with irradiation time: They become more elongated and assemble in necklaces. This reshaping might be due to heating of the Au-NPs by plasmon excitation and to reactions (which are probably catalyzed by the plasmon) at the surface of nanoparticles leading to deligandation of the citrate ions and to chemical complexation of Au with cyanide. These phenomena depend on the initial size of the Au-NPs. Indeed, in the case of the initial 15 nm Au-NPs@citrate, the UV-visible spectra do not exhibit a new plasmon band, which could correspond to elongated nanoparticles or their assembly, in contrast to what is observed for 30 nm Au-NPs@citrate. This suggests that for the initial smallest 15 nm Au-NPs@citrate, assembly and precipitation of the elongated Au-NPs take place rapidly in seconds or minutes (at the scale of the record of the spectra), while for the initial 30 nm Au-NPs@citrate, smaller aggregates are formed and remain in suspension.

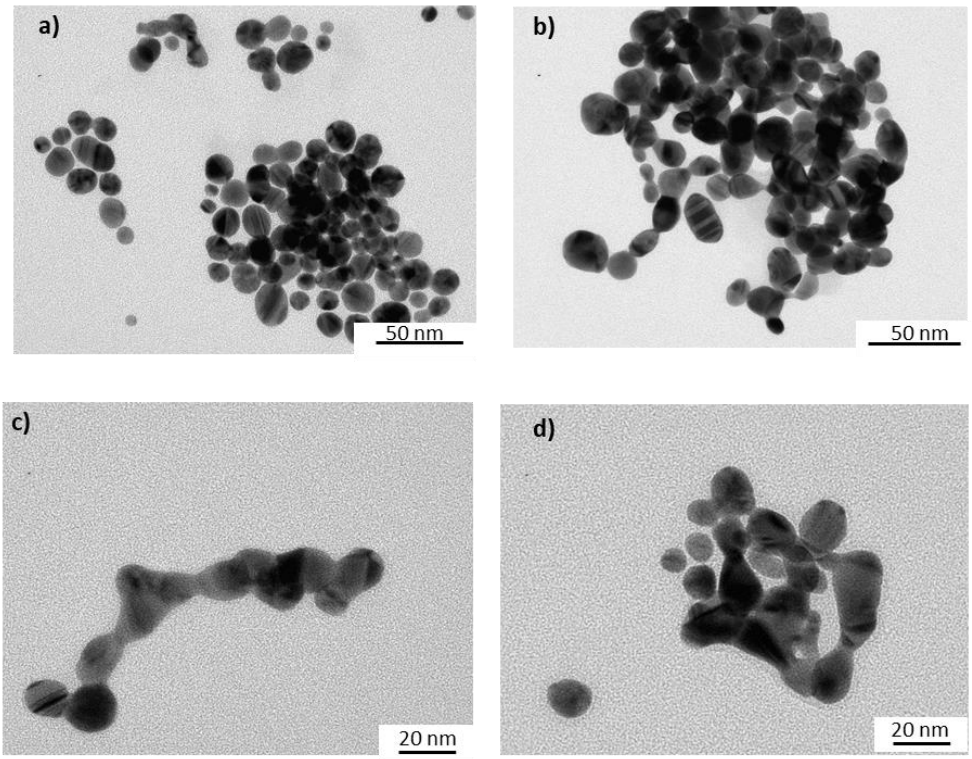

Figure 5. TEM images of the initial **15 nm** Au-NPs@citrate taken at different times during the reduction reaction of hexacyanoferrate (III) by sodium thiosulfate under irradiation with a Xe lamp equipped with a cutoff filter at 450 nm: (**a**) before irradiation, after (**b**) 30 minutes, (**c**) 120 minutes, and (**d**) 180 minutes of irradiation.

Peer-reviewed version available at *Materials* **2019**, *12*, 3012; doi:10.3390/ma12183012

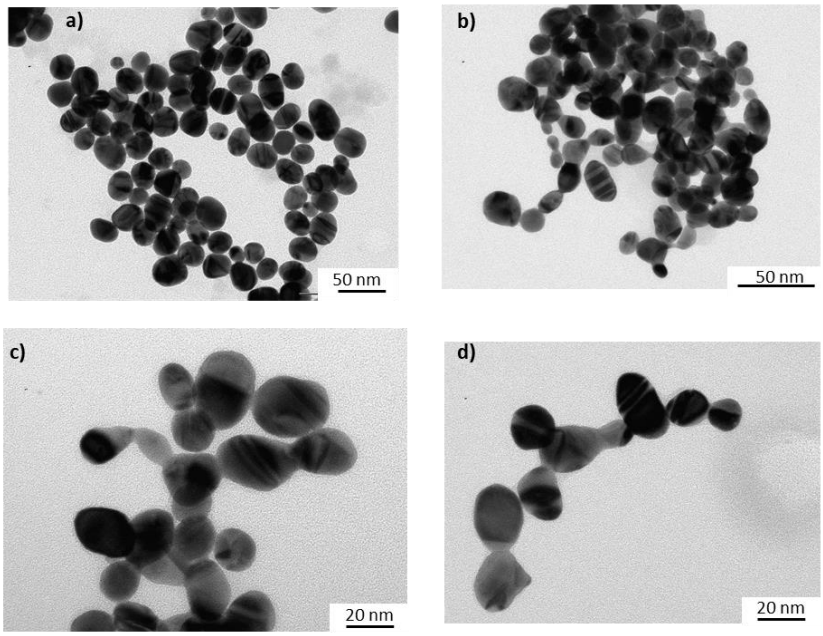

Figure 6. TEM images of initial 30 nm Au-NPs@citrate taken at different times of irradiation during the reduction reaction of hexacyanoferrate (III) by sodium thiosulfate under irradiation with a Xe lamp equipped with a cutoff filter at 450 nm: (**a**) before irradiation, and after (**b**) 30 minutes, (**c**) 120 minutes, and (**d**) 180 minutes of irradiation.

3.2. Reduction of hexacyanoferrate in the absence of sodium thiosulfate

3.2.1 Irradiation using LEDs at λ = 520 nm

Irradiation of solutions containing HC-FeIII and Au-NPs@citrate, but without ST leads to a decrease in the absorption bands at 310 and 420 nm associated to HC-FeIII as well as a decrease in the LSPR of the Au-NPs around 520 nm (Figure 7). However, that evolution is very slow compared to the changes observed in the presence of ST: While the total reduction of HC-FeIII occurs in less than 1 hour with ST (Figures 3), hardly anything happens for 2 hours without ST (Figure 8). However, the decrease in absorbance is faster for the 15 nm Au-NPs@citrate than for 30 nm Au-Nps@citrate (Figure 9). It is to note that in the dark a tiny decrease in absorbance is observed indicating the absence of reaction and the stability of the solution without irradiation (Figure S3).

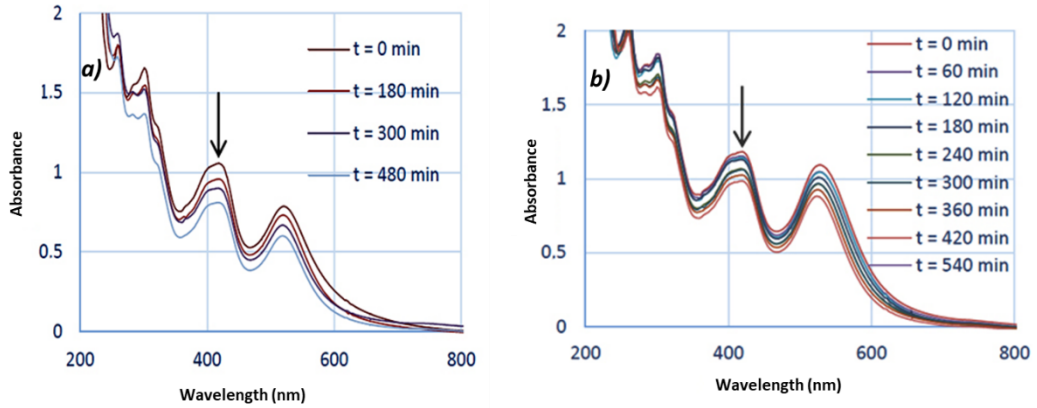

Figure 7. Spectral evolution with time of deaerated aqueous solutions containing 10^{-3} M potassium hexacyanoferrate under LEDs irradiation at 520 nm (**a**) in the presence of 15 nm Au-NPs@citrate and (**b**) 30 nm Au-NPs@citrate. Optical path length: 1 cm.

Peer-reviewed version available at Materials 2019, 12, 3012; doi:10.3390/ma12183012

The absorbance changes observed under irradiation indicate that reactions occur, which are related to the reduction of HC-FeIII. We show here that this reduction takes place even without a reducing agent such as thiosulfate or borohydrate. In the presence of TS, the reaction is faster and TS plays a role of electron relay. Without TS, the reduction reaction is probably due to hot electrons produced by plasmon excitation or by the reaction with citrate, which can be favored because of the temperature increase on the Au-NP surface subsequent to plasmon excitation. The involvement of citrate ions in the reduction reaction would lead to a loss of stabilizing agents for the Au-NPs, hence the observed change in the LSPR band.

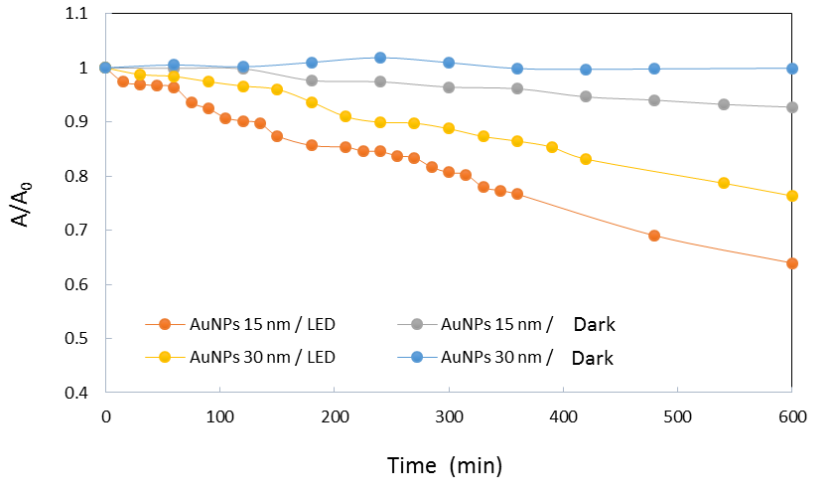

Figure 8. Kinetic traces of the normalized absorbance at 420 nm of HC-FeIII in deaerated aqueous solutions containing 10^{-2} M potassium hexacyanoferrate in the presence of 15 nm or 30 nm Au-NPs@citrate and in the dark or under LEDs irradiation at 520 nm.

3.2.2 Irradiation using a Xe lamp equipped with a 450 nm optical cutoff filter

Figure 9 presents the spectral evolution of a deaerated solution containing HC-FeIII and 15 nm Au-NPs@citrate under irradiation by a Xe lamp with a longpass filter at 450 nm. As in the case of the LED irradiation (Figure 8), a decrease in the absorbance of the bands at 310, 420 and 520 nm is observed, but this decrease is much faster since after 3 hours, the bands are almost vanished. However, comparison between Figure 4a and Figure 9 indicates that the presence of ST accelerates the spectral evolution recorded under Xe lamp irradiation and consequently the reaction. But even without ST, reshaping and precipitation due to aggregation of Au-NPs@citrate proceed.

Peer-reviewed version available at *Materials* **2019**, *12*, 3012; doi:10.3390/ma12183012

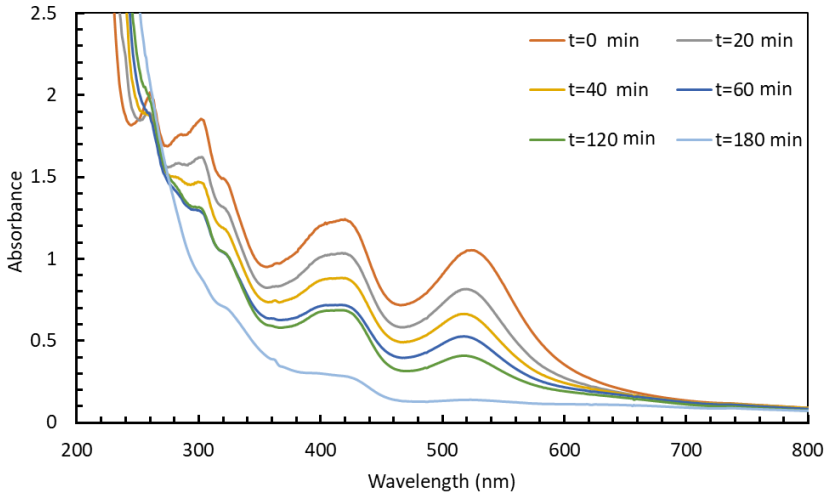

Figure 9. Spectral evolution with time of a deaerated aqueous solution containing 10^{-2} M potassium hexacyano ferrate in the presence of 15 nm Au-NPs@citrate under Xe lamp irradiation (equipped with an optical cutoff filter at 450 nm). Optical path length: 1 cm.

3.2.3 Effect of stabilizing agent of the Au-NPs

In the light of the results presented above, we repeated the experiments using Au-NPs stabilized by a non-reducing agent, and so we replaced citrate by *para*-nitrothiophenol (pNTP) since thiol based compounds are known to be used as stabilizing agents of gold nanoparticles, due to the strong affinity between sulfur and gold atoms. However, it is to keep in mind that during the reaction, the stabilizing agent (pNTP) could also transform [33], and lead to the formation of *para*-aminothiophenol (pATP), but without significant change in the stabilization of the Au-NPs [34][32].

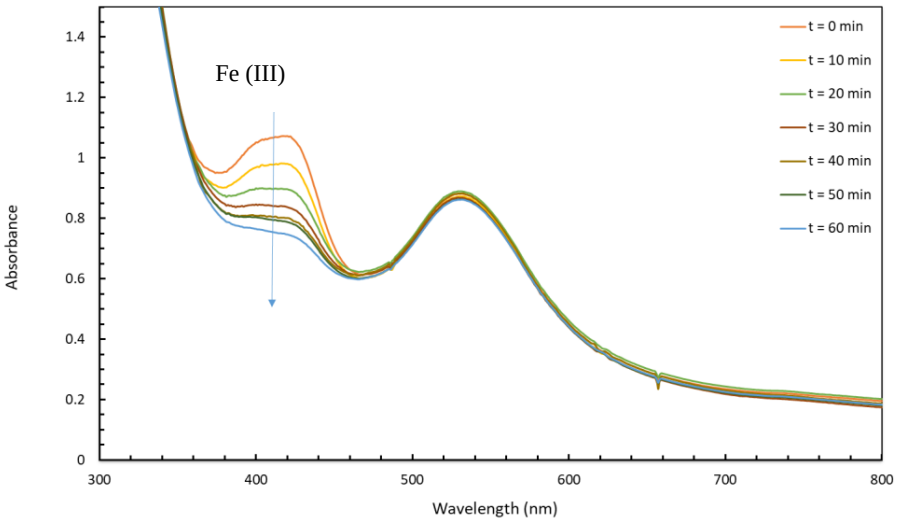

Figure 10. Spectral evolution with time of deaerated aqueous solutions containing 10^{-3} M potassium hexacyanoferrate in the presence of 15 nm Au-NPs@pNTP under LEDs irradiation at 520 nm (Optical path length: 1 cm).

Figure 10 shows the temporal evolution of the UV-visible spectrum of a deaerated solution containing 15 nm Au-NPs@pNTP and HC-FeIII under LEDs irradiation at 520 nm. In that case, while

Peer-reviewed version available at Materials 2019, 12, 3012; doi:10.3390/ma12183012

the band at 420 nm due to HC-FeIII drops, no change is observed in the LSPR band of the Au-NPs. That indicates that the 15 nm Au-NPs@pNTP are stable during the reaction under irradiation, what is confirmed by TEM images (Figure 11). It is also worth to notice that the disappearance of the absorption band due to Hc-FeIII is quite rapid, nearly as fast as in the presence of ST (Figure 2c). That proves that, even without a reducing agent such as ST, reduction of HC-FeIII occurs via plasmon excitation of Au-NPs, and consequently hot electrons are involved.

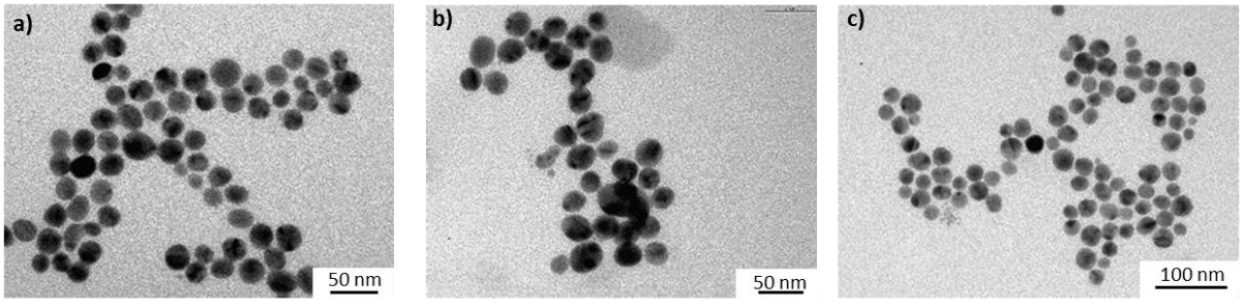

Figure 11. TEM images of initial 15 nm Au-NPs@pNTP taken at different times during the reduction reaction of hexacyanoferrate (III) under LEDs irradiation at 520 nm: (**a**) 10 minutes, (**b**) 30 minutes, and (**c**) 60 minutes of irradiation.

4. Discussion

The previous results show the disappearance of HC-FeIII catalyzed by Au-NPs under irradiation in the presence, or not of ST. This disappearance is attributed to the reduction of HC-FeIII. To confirm the reaction and to have some insights into the role played by Au-NPs, XPS analysis were carried out to determine the oxidation states of iron and gold.

The XPS wide-scan spectra of 30 nm Au-NPs@citrate after reaction under LEDs irradiation at 520 nm for deaerated solutions containing HC-FeIII with ST or without ST (Figure S4) show the presence of gold, iron, carbon, nitrogen, oxygen, potassium and sodium. Oxygen and carbon are due to citrate ions at the surface of the Au-NPs; Sodium can be related to sodium citrate but also to sodium thiosulfate when present, and potassium and nitrogen comes from potassium hexacyanoferrate. Figure 12 presents the XPS spectra recorded for the Au4f, Fe2p and N1s regions.

Preprints (www.preprints.org) | NOT PEER-REVIEWED | Posted: 17 July 2019 doi:10.20944/preprints201907.0197.v1

Peer-reviewed version available at Materials 2019, 12, 3012; doi:10.3390/ma12183012

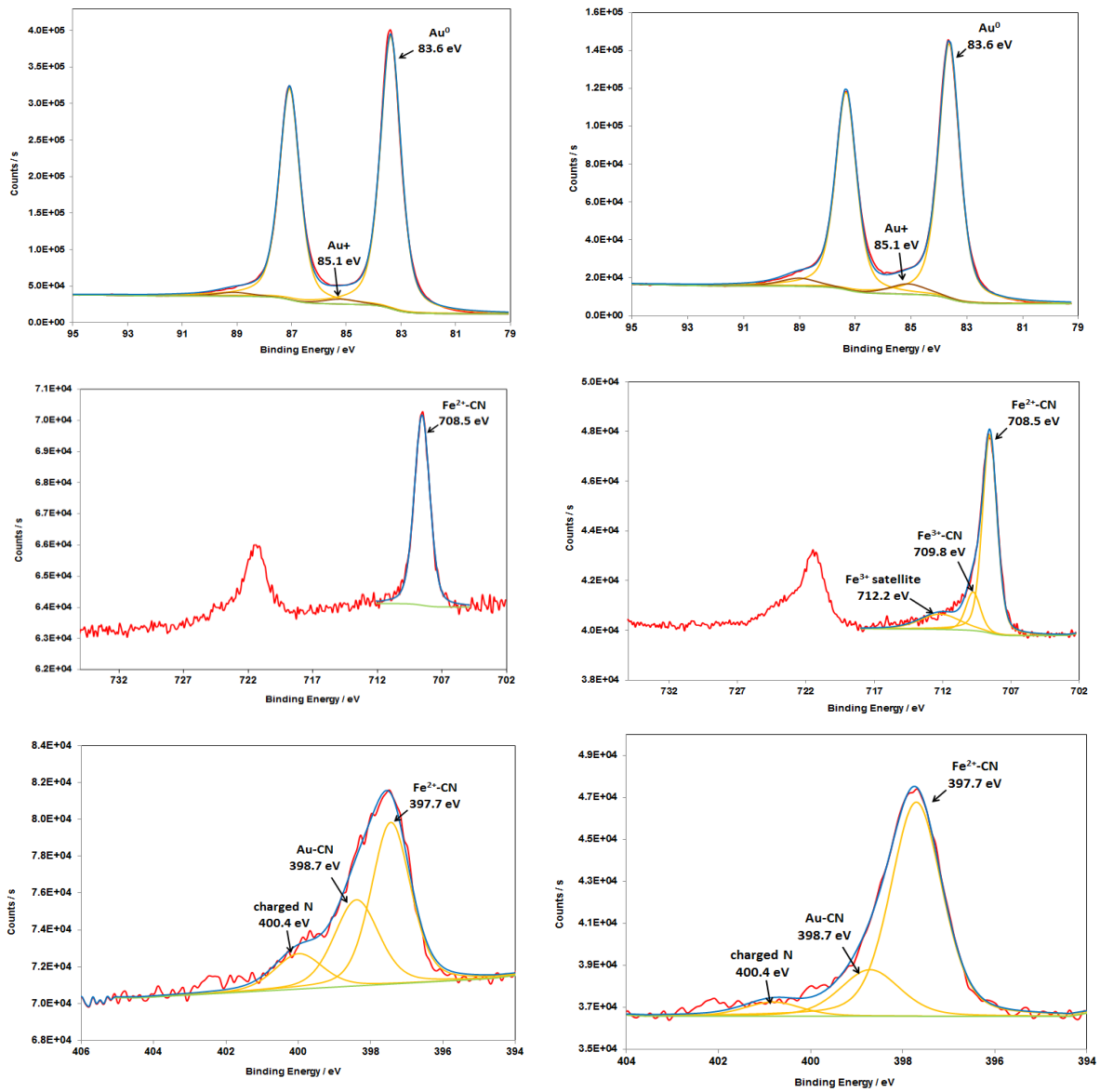

Figure 12. XPS spectra of Au4f (a,b), Fe2p (c,d) and N1s (e,f) core levels of 30 nm-Au-NPs@citrate after reaction after reaction under LEDs irradiation at 520 nm (during 60-minutes) for deaerated solutions containing hexacyanoferrate (a,c,e) with or (b,d,f) without sodium thiosulfate.

The main Au4f signals appear as a doublet separated by 3.7 eV with $Au4f_{7/2}$ and $Au4f_{5/2}$ peaks at 83.6 and 87.3 eV, respectively.[35], what are characteristic values of binding energies for metallic Au atoms (Figure 12 a and 12 b). In the case of the sample without ST, a second doublet is identified at 85.1eV and 89.0 eV (Figure 13b) which can be attributed to Au-CN bounds [36,37] rather than to Au-citrate [37-39]. This assumption is supported by the presence of a contribution at 398.7 eV in the N1s spectrum (Figure 12 f), which has an area equivalent to that of Au^+ in Au4f [36] . This component at 85.1 eV is also present in the Au4f core-level spectrum of the sample with ST (Figure 12 a) but to a lesser extent, proving that Au is more protected from oxidation when ST is present. Investigations of Fe2p core-level spectra corroborate further the effect of ST. A complete reduction of Fe^{III} into Fe^{II} is observed in the presence of thiosulfate (Figure 12 c), while in the absence of thiosulfate, only 84% of Fe^{III} has been reduced (Figure 12 d). In Figure 12 c Fe^{II} is easily identified by the presence of a single doublet located at 708.5 ($Fe2p_{3/2}$) and 721.5 eV ($Fe2p_{1/2}$), typical values for $K_3[Fe(CN_6)]$ [40]. This result confirms the hypothesis that, in the presence of ST, at the end of the reaction (after LEDs

Peer-reviewed version available at Materials 2019, 12, 3012; doi:10.3390/ma12183012

irradiation for 60 min), there is a complete reduction of Fe^{III} into Fe^{II} in the present experimental conditions. The presence of a second doublet at 709.8 and 723.7 eV in the spectrum of the sample without ST (Figure 12 d) is indicative of Fe^{III} [41,42]. The N1s core-level spectrum was decomposed into three contributions, one corresponding to nitrogene in CN bridges, at 397.7 eV, a second contribution at 398.6 eV, which can be attributed to AuCN [29] and a small contribution at 400.4 eV corresponding to charged nitrogen.

Furthermore, the components attributed to AuCN (in the sample with or without ST) shows that the reaction takes place at the surface of Au-NPs@citrate, leading to an oxidation of Au atoms and ligation of Au-NPs@citrate to CN^-. This might account for the small changes observed in the LSPR of Au-NPs@citrate in presence of ST and the decrease in LSPR band (Figure S7), oxidation being more effective in that case. Indeed, cyanides are used to extract gold from mines by its oxidation and complexation [43]. CN^- has a great ability to complex with Au and form a stable complex $Au(CN)_2^-$:

$$2\ Au + 4\ CN^- + O_2 + 2\ H_2O \rightarrow 2\ Au(CN)_2^- + 2\ OH^- \quad (1)$$

The Gibbs free energy of the reaction (1) is −315.7 kJ, indicating that the reaction is spontaneous. In TEM images, observation of small clusters of Au indicate this partial dissolution. Similar dissolution by cyanide ions has already been invoked in the case of size reduction and reshaping of Pt NPs used as catalysts for electron transfer reaction between hexacyanoferrate and thiosulfate [21,22]

To summarize, in the presence of ST Au is much less oxidized than in the absence of ST, because in the former case Au-NPs@citrate work mainly as catalysts in the electron transfer from thiosulfate to Fe^{III}. When ST is not present, the reduction of Fe^{III} occurs as shown by UV-visible spectra and XPS analysis. This reduction takes place either by hot electrons induced by plasmon excitation of Au-NPs, or by citrate. In the former case, the electrons are mainly transferred from Au NPs to Fe^{III}, leading to Au^I, which will probably be ligated to CN^- present in the solution. The reduction of Fe^{III} may also be partly due to reduction by citrate, which may become possible because of the temperature increase around the Au-NPs@citrate due to the plasmonic photothermal conversion.

5. Conclusions

Plasmonic catalysis enables to achieve reactions using solar light with less energy and time consumption. The reduction kinetics of ferricyanide (III) ion into ferrocyanide (II) by Au-NPs is enhanced under visible light excitation. This reduction takes place even without sodium thiosulfate and is due to transfer of hot electrons induced by plasmon excitation. The Au-NPs stabilized by citrate reshape during the reaction. However, the shape of the Au-NPs remains stable when they are stabilized by stronger ligands such as *para*-nitrophenol, and the Au-NPs could then be reused in different catalytic cycles.

This study shed some light on the possible direct applications of catalysis assisted by plasmon of gold nanoparticles excited by visible light. The results demonstrate the effectiveness of using colloidal spherical gold nanoparticles to catalyze redox reactions under visible irradiation.

Supplementary Materials: The following are available online at www.mdpi.com/xxx/s1, Figure S1: LED reactor; Figure S2: UV-visible spectra of HC-FeIII and ST; Figure S3: Spectral evolution with time of deaerated aqueous solutions containing 10^{-3} M potassium hexacyanoferrate in the dark in the presence of Au-NPs@citrate Figure S4: XPS wide scan spectra of 30 nm-Au-NPs@citrate after reaction after reaction under LEDs irradiation at 520 nm for deaerated solutions containing hexacyanoferrate (A) with or (C) without sodium thiosulfate.

Author Contributions: I.S. worked on the Au-NPs synthesis, catalytic studies and data treatment and contributed to the writing of the manuscript. P.B. carried out the TEM analysis. D.D. performed the XPS analysis. P.B. participated in discussing the plasmon effect. I.L. and H.R. conducted the project, worked on the analysis of the data and wrote the paper.

Funding: This research was funded by C'Nano IdF.

Acknowledgments: IS acknowledge the financial support of C'Nano IdF and DIM NanoK.

Conflicts of Interest: The authors declare no conflict of interest.

References

1. Krishnendu, S.; Agasti, S.S.; Chaekyu, K.; Xiaoning, L.; Rotello, V.M. Gold nanoparticles in chemical and biological sensing. *Chem. Rev.* **2012**, *112*, 2739-2779.
2. Lang, X.; Chen, X.; Zhao, J. Heterogeneous visible light photocatalysis for selective organic transformations. . *Chem. Soc. Rev.* **2014**, *43*, 473-486.
3. Haruta, M.; Kobayashi, T.; Sano, H.; Yamada, N. Novel Gold Catalysts for the Oxidation of Carbon Monoxide at a Temperature Far Below 0 °C. *Chem. Lett* **1987**, *37*, 1290 - 1291.
4. Zanella, R.; Giorgio, S.; Shin, C.; Henry, C.; Louis, C. Characterization and reactivity in CO oxidation of gold nanoparticles supported on TiO2 prepared by deposition-precipitation with NaOH and urea. *J. Catal.* **2004**, *222*, 357-367.
5. Huang, X.; Neretina, S.; El-Sayed, M. Gold Nanorods: From Synthesis and Properties to Biological and Biomedical Applications. *Adv. Mater.* **2009**, *21*, 4880-4910.
6. Vincenzo; Amendola, e.a. Surface plasmon resonance in gold nanoparticles: a review. . *J Phys Condens Matter.* **2017**, *29*.
7. Zhang, J.; Wang, L.; Ali, S.; Wang, C.; Wang, L.; Meng, X.; Li, B.; Su, D.; Xiao, F. Wet-Chemistry Strong Metal-Support Interactions in Titania-Supported Au Catalysts. *ACS* **2019**, *141*, 2975-2983.
8. Dohyung, K.; Joaquin, R.; Yi, Y.; Asiri, A.M.; Peidong, Y. Synergistic geometric and electronic effects for electrochemical reduction of carbon dioxide using gold–copper bimetallic nanoparticles. . *Nature. Comm.* **2014**, *5*, 4948.
9. Abidi, W.; Selvakannan, P.; Guillet, Y.; Lampre, I.; Beaunier, P.; Pansu, B.; Palpant, B.; Remita, H. One-Pot Radiolytic Synthesis of Gold Nanorods and Their Optical Properties. . *J. Phys. Chem. C* **2010**, *114*.
10. Linic, S.; Christopher, P.; Ingram, D.B. Plasmonic-Metal Nanostructures for Efficient Conversion of Solar to Chemical Energy. *Nat. Mater.* **2011**, *10*, 911-921.
11. Kim, K.; Lee, I.; Lee, S.J. Photocatalytic reduction of 4-nitrobenzenthiol on Au mediated via Ag nanoparticles. . *Chem. Phys. Lett.* **2003**, *377*, 201-204.
12. Hong, S.; Li, X. Optimal Size of Gold Nanoparticles for Surface-Enhanced Raman Spectroscopy under Different Conditions. *Journal of Nanomaterials* **2013**, *2013*, 1-9.
13. Kowalska, E.M., O.O; Abe, R; Ohtani, B. Visible-light-induced photocatalysis through surface plasmon excitation of gold on titania surfaces. *Physical chemistry chemical physics : PCCP* **2010**, *12*, 2344-2355.
14. Méndez-Medrano, M.G.K., E; Lehoux, A; Herissan, A; Ohtani, B; Bahena, D; Briois, V; Colbeau-Justin, C; Rodríguez-López, J.L; Remita, H. Surface Modification of TiO2 with Ag Nanoparticles and CuO Nanoclusters for Application in Photocatalysis. *J. Phys. Chem. C* **2016**, *120*, 5143-5154.
15. Wang, C.; Astruc, D. Nanogold plasmonic photocatalysis for organic synthesis and clean energy conversion. *Chem. Soc. Rev.* **2014**, *43*, 7188-7216.

Peer-reviewed version available at Materials 2019, 12, 3012; doi:10.3390/ma12183012

16. Huang, X.; El-Sayed, M.A.; El-Sayed, I.H.; Qian, W. Cancer cell imaging and photothermal therapy in the near-infrared region by using gold nanorods. . *J. Am. Chem. Soc.* **2006**, *128*, 2115-2120.

17. Loo, C.; Lin, A.; Hirsch, L.; Lee, M.H.; Barton, J.; Halas, N.; West, J.; Drezek, R. Technology in Cancer Research & Treatment. *ISSN* **2004**, *1533-0346*, 33-40.

18. Xiaohua, H.; Ivan, H., El-Sayed. ; Qian., W.; El-Sayed, M.A. Cancer Cell Imaging and Photothermal Therapy in the Near-Infrared Region by Using Gold Nanorods. *J. Am. Chem. Soc.* **2006**, *128*, 2115.

19. Rong, H.; Y, C.W.; Xiaoyong, W.; Gang, L.; Wei, Z.; Longping, W.; Chen., X.; Kie, Z.; Hou, J.G. Facile synthesis of pentacle gold-copper alloy nanocrystals and their plasmonic and catalytic properties. *Nature Comm.* **2014**, 1-10.

20. Labouret, T.; Audibert, J.-F.; Pansu, R.B.; Palpant, B. Plasmon-Assisted Production of Reactive Oxygen Species by Single Gold Nanorods. *Small* **2015**, *11*, 4475-4479, doi:10.1002/smll.201500509.

21. Narayanan, R.; El-Sayed, M.A. Effect of Catalytic Activity on the Metallic Nanoparticle Size Distribution: Electron-Transfer Reaction between Fe(CN)6 and Thiosulfate Ions Catalyzed by PVP−Platinum Nanoparticles. *J. Phys. Chem.* **2003**, *107*, 12416–12424.

22. Yen, C.W.; El-Sayed, M.A. Plasmonic field effect on the hexacyanoferrate (III)-Thiosulfate electron transfer catalytic reaction on gold nanoparticles: Electromagnetic or Thermal? . *J. Phys. Chem. C.* **2009**, *113*, 19585-19590.

23. Carregal-Romero, S.; Perez-Juste, J.; Herves, P.; Liz-Marzan, L.M.; Mulvaney, P. Colloidal gold-catalyzed reduction of ferrocyanate (III) by borohydride ions: a model system for redox catalysis. *Langmuir : the ACS journal of surfaces and colloids* **2010**, *26*, 1271-1277.

24. Narayanan, R.; El-Sayed, M.A. Shape-Dependent Catalytic Activity of Platinum Nanoparticles in Colloidal Solution. *Nano Lett.* **2004**, *4*, 1343–1348.

25. El-Sayed, N.a.M.A. Shape-Dependent Catalytic Activity of Platinum Nanoparticles in Colloidal Solution. *Nano Letters* **2004**, *4 (7)*.

26. Radha Narayanan; El-Sayed, M.A. Shape-Dependent Catalytic Activity of Platinum Nanoparticles in Colloidal Solution. *Nano Letters* **2004**, *4 (7)*.

27. Wang, C.; Astruc, D. Photocatalysis for Organic Synthesis and Clean Energy Conversion. *Chem. Soc. Rev* **2014**, *43*, 7188–7216.

28. I.Sarhid; I.Abdellah; Lampre, I.; Huc, V.; Martini, C.; Remita, H. Plasmonic catalysis for the Suzuki–Miyaura cross-coupling reaction using palladium nanoflowers. *New J. Chem* **2019**, *43*, 4349-4355

29. Turkevich, J.; Stevenson, P.; Hillier, J. A study of the nucleation and growth processes in the synthesis of colloidal gold. *Discuss Faraday Soc.* **1951**, *11*, 55-57.

30. Pluchery, O.; Remita, H.; Schaming, D. Demonstrative experiments about gold nanoparticles and nanofilms: an introduction to nanoscience. *Gold Bulletin* **2013**, *46*, 319-327.

31. Schaming, O.P.H.R.D. Demonstrative experiments about gold nanoparticles and nanofilms: an introduction to nanoscience. *Gold Bulletin* **2013**, *46*, 319-327.

32. Rumble, J.R.L., David R; Bruno, Thomas J. *CRC handbook of chemistry and physics* 2017.

33. Woehrle, G.H.; Brown, L.O.; Hutchison, J.E. Thiol-functionalized, 1.5-nm gold nanoparticles through ligand exchange reactions: scope and mechanism of ligand exchange. *Journal of the American Chemical Society* **2005**, *127*, 2172-2183.

34. Zhao, L.B.; Zhang, M.; Huang, Y.F.; Williams, C.T.; Wu, D.Y.; Ren, B.; Tian, Z.Q. Theoretical Study of Plasmon-Enhanced Surface Catalytic Coupling Reactions of Aromatic Amines and Nitro Compounds. *J. Phys. Chem. Lett.* **2014**, *5*, 1259-1266.

35. Yuan, L.; Wenwu, S.; Aditya, G.; Nitin, C. Morphological evolution of gold nanoparticles on silicon wires and their plasmonics. *RSC Adv.* **2015**, *5*, 49708-49718.

36. Cook, R.; Crathorne, E.A.; Monhemius, A.J.; Perry, D.L. XPS Study of the Adsorption of Gold (I) Cyanide by Carbons. *Hydrometallugy.* **1989**, *22*, 171-182.

37. Park, J.W.; Shumaker-Parry, J.S. Structural Study of Citrate Layers on Gold Nanoparticles : Role of Intermolecular Intercations in Stabilizing Nanoparticles. *J. Am. Chem. Soc.* **2014**, *163*, 1907-1921.

38. ZHuo, C.K.; Huang, X.; Zhang, P.Y. Sub-Two Nanometer Single Crystal Nanowires. *Nano Lett.* **2008**, *8*, 2041-2044.

39. Mikhlin, Y.; Likhatski, M.; Karacharov, A.; Zaikowski, V.; Krylov, A. Formation of gold and gold sulfide nanoparticles and mesosclae intermediate structures in the reactions of aqueous HAuCl4 with sulfide and citrate ions. *Phys. Chem. Chem. Phys.* **2009**, *11*, 5445-5454.

40. Naumkin, A.V.; Kraut-Vass, A.; Gaarenstroom, S.W.; Powell, C.J. NIST X-ray Photoelectron Spectroscopy Database, NIST Standard Reference Database. *National Institute of Standards and Technology (NIST)* **2000**, *20899*.

41. Stefaans, J.G.; Erasmus, E. Electronic effects of metal hexacyanoferrates : An XPS and FTIR study. *Mater. Chem. Phys.* **2018**, *203*, 73-81.

42. Grosvenor, A.P.; Kobe, B.A.; Biesinger, M.C.; McIntyre, N.S. Investigation of multiplet splitting of Fe 2p XPS spectra and bonding in iron compounds. *Surf. Interf. Anal.* **2004**, *36*, 1564-1574.

43. Wang, J.; Lu, Y.; Xu, Z. Identifying Extraction Technology of Gold from Solid Waste in Terms of Environmental Friendliness. *ACS Sustainable Chemistry & Engineering* **2019**, *7*, 7260-7267.